Magnetic neutron diffraction study of the charge-ordered chain compounds $Rb_{11}Mn_8O_{16}$ and $Cs_3Mn_2O_4$

M. Reehuis,[1] M. A. Señaris-Rodriguez,[2,3] A. Hoser,[1] B. Keimer,[2] and M. Jansen[2]
[1]*Helmholtz-Zentrum Berlin für Materialien und Energie, D-14109 Berlin, Germany*
[2]*Max Planck Institute for Solid State Research, Heisenbergstrasse 1, D-70569 Stuttgart, Germany*
[3]*Departamento Química Fundamental, Facultad de Ciencias Universidad de A Coruña, E-15071 A Coruña, Spain*
(Received 28 November 2012; published 24 January 2013)

The magnetic ordering patterns of $Rb_{11}Mn_8O_{16}$ and $Cs_3Mn_2O_4$ were determined by neutron powder diffraction with and without applied magnetic fields. The crystal structures of these compounds exhibit infinite chains of edge-sharing MnO_4 tetrahedra with periodically alternating Mn^{2+} and Mn^{3+} valence. Both $Rb_{11}Mn_8O_{16}$ and $Cs_3Mn_2O_4$ show collinear magnetic order with antiferromagnetic alignment of Mn moments along the chains below the Néel temperatures $T_N = 38(1)$ and 13.5(5) K, respectively. In $Cs_3Mn_2O_4$ the Mn^{2+} and Mn^{3+} moments could be separately refined. The full magnetic structure in a zero magnetic field can be viewed as a set of ferrimagnetic chains whose net moments are coupled antiferromagnetically perpendicular to the chain direction. For this compound, we further observe a magnetic field induced transition into a high-field phase with uniformly aligned ferrimagnetic moments.

DOI: 10.1103/PhysRevB.87.014426 PACS number(s): 61.05.fm, 61.66.Fn

I. INTRODUCTION

Multinary oxides provide a highly diverse platform for the investigation of collective order and transport phenomena in correlated-electron systems. However, the delicate sensitivity of correlated-electron systems to disorder, in combination with ubiquitous random perturbations of the spatially periodic crystal structure of real materials, has created formidable challenges for research in this field. In copper oxides with spin-liquid (Ref. 1) or superconducting (Ref. 2) ground states, for instance, controlled substitution of a dilute concentration of impurities was observed to nucleate competing antiferromagnetic order on the nanoscale. Yet random chemical substitution is still the method of choice to systematically alter the valence state of transition-metal ions in a given compound family, and the uncontrolled disorder generated in this way greatly complicates the microscopic understanding of their physical properties. The synthesis of intrinsically doped compounds with fully periodic lattices of metal ions in alternating valence states has recently opened up new perspectives for the investigation of collective electronic order in the absence of chemical and structural disorder. These include manganates with double-perovskite structure with ordered arrays of Mn^{3+} and Mn^{4+} ions (Ref. 3), as well as sodium cuprates with strands of edge-sharing CuO_4 squares containing periodic lattices of copper ions in formal valence states Cu^{2+} and Cu^{3+}.[4–8]

As a similarly prolific class of compounds, alkali manganates (II/III) of general composition A_xMnO_2 (A = K, Rb, and Cs) (Refs. 9–13) have recently become available through the azide/nitrate synthesis route.[14,15] Together with $Na_{26}Mn_{39}O_{55}$ (Ref. 16) and $LiMn_3O_4$ (Ref. 17), this new series constitutes one of very few examples of ternary manganese II/III mixed valent compounds, in contrast to the vast number of existing manganate (III/IV) mixed oxides. In addition, the synthetic procedure can be scaled up to gram amounts, and it allows precise and reproducible determination of the degree of transition-metal doping. Some of these new alkali manganates (such as $K_{29}Mn_{17}O_{34}$) show commensurably modulated structures; others (including $Rb_{15}Mn_{11}O_{22}$) exhibit incommensurate structures.[11,12] They all share the same basic architecture featuring doped MnO_2 chains of *trans*-edge-sharing tetrahedra, which are arranged in a honeycomb pattern and are centering hexagonal channels. The walls of the channels are decorated with the alkali ions. As a consequence, the magnetic interactions are highly anisotropic.

Here we report a neutron powder diffraction study of two recently synthesized members of this family, $Rb_{11}Mn_8O_{16}$ (Refs. 11 and 12) and $Cs_3Mn_2O_4$ (Ref. 13), with Mn in the average formal oxidation state of 2.625+ and 2.50+, respectively. The study of their magnetic structures by means of neutron powder diffraction is challenging in view of their complex crystal structures. As reported in Ref. 11, $Rb_{11}Mn_8O_{16}$ crystallizes in the space group $F222$, with cell parameters $a = 1220.96(4)$ pm, $b = 2015.95(7)$ pm, and $c = 4371.2(2)$ pm. This unit cell contains 128 manganese ions, located at 17 different sites, in a sometimes heavily distorted oxide tetrahedral environment. The edge-sharing MnO_4 tetrahedra give rise to two types of screwed MnO_2 chains that run parallel to the c axis of the orthorhombic structure. These are separated by rubidium ions which form a distorted honeycomblike arrangement of channels (Fig. 1). Chains of type I contain Mn ions located at nine different Wyckoff positions, namely, Mn1 at $4a(0,0,0)$, Mn2 at $4b(0,0,1/2)$, Mn3–Mn9 at $8g(0,0,z)$, while chains of type II contain Mn ions located at eight other different Wyckoff positions: Mn10–Mn17 at $8h(1/4,1/4,z)$.[11] Along the chains the interatomic oxygen-manganese distances show a significant spread from 1.84 to 2.06 Å (covering the range expected for Mn^{2+} and Mn^{3+} distances to oxygen). In a picture based on integral charges localized at the Mn ions, the average formal charge per manganese ion in $Rb_{11}Mn_8O_{16}$ would imply three Mn^{2+} and five Mn^{3+} ions per formula unit (i.e., $Rb_{11}Mn^{2+}{}_3Mn^{3+}{}_5O_{16}$). However, the real charge distribution is smoother and resembles the one observed for charge density waves in metals.[12] In view of its complexity, the crystal structure of this compound is best described

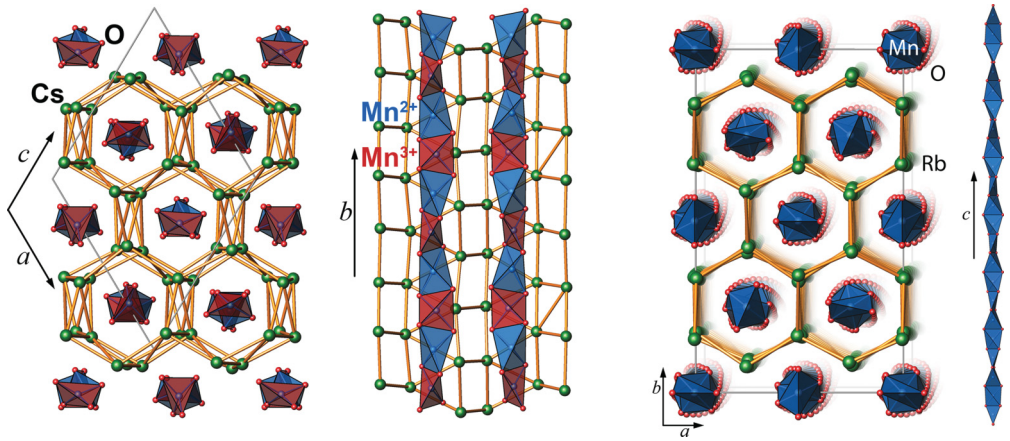

FIG. 1. (Color online) Perspective representation of the crystal structures of $Cs_3Mn_2O_4$ (left) and $Rb_{11}Mn_8O_{16}$ (right).

as an incommensurate composite structure, built up of two interpenetrating substructures: a honeycomblike framework of Rb ions as one subsystem, and the manganate chain polyanions as a second subsystem.[12]

The closely related crystal structure of $Cs_3Mn_2O_4$ [$P2_1/c$, cell parameters: $a = 1276.33(1)$ pm, $b = 1082.31(2)$ pm, $c = 1280.29(2)$, and $\beta = 118.390(2)$] is comparatively simple.[13] Its unit cell is smaller and contains 16 Mn ions at four different sites, all at the Wyckoff position $4e(x,y,z)$. In this case, the MnO_2 infinite chains, which are also built up of edge-sharing MnO_4 tetrahedra, run along the b axis (Fig. 1). In contrast to $Rb_{11}Mn_8O_{16}$, the four structurally different Mn atoms (Mn1–Mn4) are found within the same chain, with ions at Mn1 and Mn2 in valence state 3+ and those at Mn3 and Mn4 in valence state 2+, and a complete charge ordering with sequence -Mn^{2+}-Mn^{3+}-Mn^{2+}-Mn^{3+}- is observed along the chains.

II. EXPERIMENTAL DETAILS

$Cs_3Mn_2O_4$ and $Rb_{11}Mn_8O_{16}$ were prepared via the azide/nitrate route from Mn_2O_3 and the respective alkali-metal nitrates and azides.[14,15] The starting materials were mixed in appropriate molar ratios and reacted according to the prescriptions given in Refs. 11, 12, and 13, respectively. The purity of the products was checked by room temperature x-ray powder diffraction using a D-8 Bruker diffractometer with Mo $K\alpha_1$ radiation ($\lambda = 0.7093$ Å) in Debye-Scherrer geometry. The magnetic properties were studied in a Quantum Design MPMS7 SQUID magnetometer. Zero-field-cooled (ZFC) and field-cooled magnetic susceptibility data were obtained under different fields 10^{-3} T $\leqslant H \leqslant 7$ T in the temperature range 4.2 K $\leqslant T \leqslant$ 350 K. Hysteresis loops with variable field up to $\pm$7 T were obtained in ZFC conditions at temperatures 2.5 K $\leqslant T \leqslant$ 300 K.

For the neutron diffraction experiments, ten product batches of 400–500 mg each were accumulated for both of the manganates investigated. The samples were pressed to cylindrical pellets and postannealed in order to prevent reorientations of individual grains in the magnetic field, and sealed under helium in quartz ampoules.

The neutron powder diffraction experiments were carried out on the instruments E6 and E9 at the BER II reactor of the Helmholtz-Zentrum Berlin, using pyrolytic-graphite and Ge monochromators selecting the neutron wavelengths $\lambda = 2.42$ Å and $\lambda = 2.795$ Å, respectively. In order to determine the temperature dependence of the ordered magnetic moments, from $T = 2$ K up to the Néel temperature T_N, 30 powder patterns were recorded for each $Rb_{11}Mn_8O_{16}$ ($Cs_3Mn_2O_4$) sample on the high-intensity neutron powder diffractometer E6 for diffraction angles between 8° and 122° (6° and 136°). In addition, the magnetic field dependence of the magnetic structure of $Cs_3Mn_2O_4$ was investigated at $T = 2$ K on the instrument E9 for $0 \leqslant H \leqslant 2.5$ T. Here the data were collected in the 2θ range between 5° and 139°. The refinements of the crystal and magnetic structure were carried out with the program FULLPROF (Ref. 18) with nuclear scattering lengths $b(O) = 5.805$ fm, $b(Mn) = -3.73$ fm, $b(Rb) = 7.08$ fm, and $b(Cs) = 5.42$ fm.[19] The magnetic form factors of the Mn^{2+} and Mn^{3+} ions were taken from Ref. 20.

III. RESULTS AND DISCUSSION

A. Sample characterization

According to conventional x-ray powder diffraction results the samples of $Cs_3Mn_2O_4$ and $Rb_{11}Mn_8O_{16}$ prepared for the present study are single phase and display the expected crystal structures. The magnetic susceptibility of these samples agrees with the one previously reported for these compounds.[11,13] The susceptibility of $Rb_{11}Mn_8O_{16}$ is small and approximately field independent, and it does not show any transition to an uncorrelated paramagnetic regime in the temperature range studied (Fig. 2). This behavior has been ascribed to strong antiferromagnetic Mn-Mn interactions along the chains.[11] In addition, χ_m shows an upward trend upon cooling for temperatures below about 40 K, which was already present in the data reported earlier.[11] The fact that it also appears in all $Rb_{11}Mn_8O_{16}$ samples prepared for the present study suggests that it is intrinsic for this compound. The neutron diffraction data reported here now allow us to associate this feature with an antiferromagnetic phase transition. The net magnetization of $\sim 0.036\mu_B$ under the maximum applied field of 7 T is much smaller than the one expected for a system with 37.5% high-spin Mn^{2+} and 62.5% Mn^{3+} ($\sim 4.4\mu_B$), consistent with strong antiferromagnetic exchange interactions between the

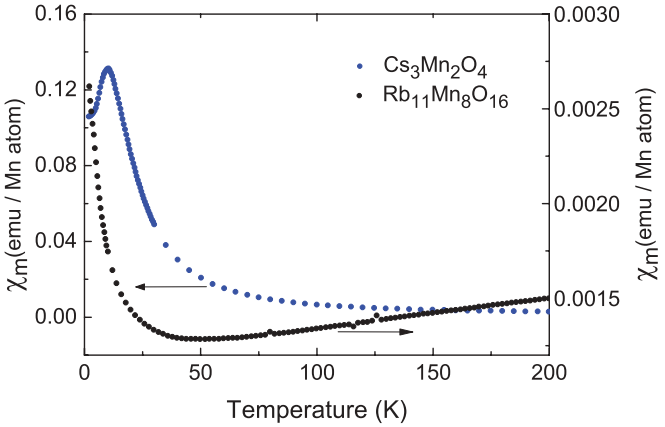

FIG. 2. (Color online) Temperature dependence of the molar magnetic susceptibility of $Rb_{11}Mn_8O_{16}$ (black) and $Cs_3Mn_2O_4$ (blue) measured for $H = 1$ T.

Mn ions. The slight hysteresis and S shape of the $M(H)$ curve shown in Fig. 3 may indicate a small ferromagnetic component of the magnetic order, consistent with the low-temperature upturn of the susceptibility upon cooling in constant field.

Measurements of the magnetic susceptibility of $Cs_3Mn_2O_4$ (Fig. 2) also showed a strong increase upon cooling at low temperatures, as well as an anomaly that confirms the previously reported antiferromagnetic transition with Néel temperature $T_N \sim 12$ K.[13] In addition, isothermal magnetization measurements as a function of field at temperatures $T < T_N$ corroborate the two-step metamagnetic transition that has also been reported previously.[13] The first step occurs at very small magnetic fields, and is followed by a second step at about 0.8 T (Fig. 3). No further transitions were observed up to 7 T. In agreement with the prior results, the net magnetization of the intermediate phase reached a value that is about 1/3 of

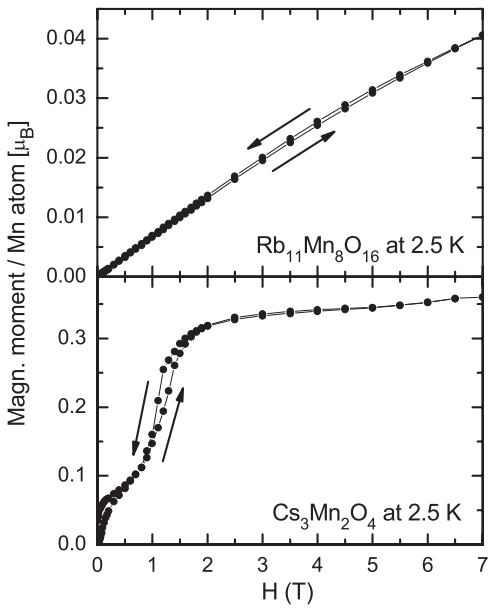

FIG. 3. Isothermal magnetization of $Rb_{11}Mn_2O_4$ and $Cs_3Mn_2O_4$ as a function of magnetic field measured at $T = 2.5$ K.

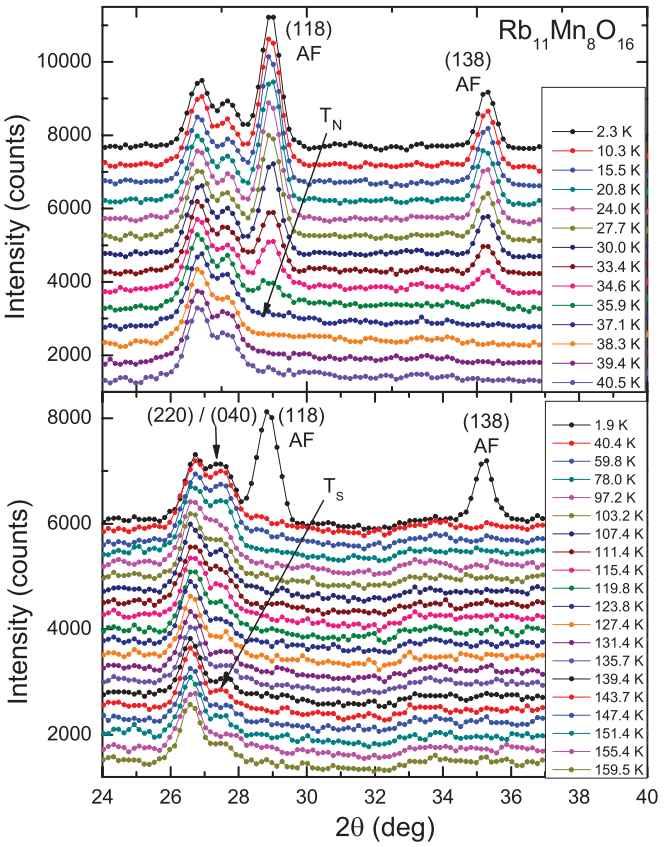

FIG. 4. (Color online) Neutron powder patterns of $Rb_{11}Mn_8O_{16}$ collected in the temperature range between 2 and 160 K. Antiferromagnetic ordering of the Mn atoms in $Rb_{11}Mn_8O_{16}$ sets in at the Néel temperature $T_N = 38(1)$ K. Magnetic intensity was also found at the position of the reflections (220) and (040), indicating a possible additional phase transition at $T_S = 140(2)$ K.

the one observed at the highest measured field (7 T), $M_{max} = 0.36\mu_B$. This value is again far below the saturation value of $4.5\mu_B$ expected for a system with 50% high-spin Mn^{2+} and 50% Mn^{3+} ions, and is therefore consistent with strong antiferromagnetic interactions.

B. Magnetic structure of $Rb_{11}Mn_8O_{16}$ and $Cs_3Mn_2O_4$

The neutron powder diffraction studies revealed antiferromagnetic ordering with Néel temperatures of $T_N = 13.5(5)$ K in $Cs_3Mn_2O_4$, and at $T_N = 38(1)$ K in $Rb_{11}Mn_8O_{16}$ (Figs. 4 and 5). The magnetic Bragg intensities were obtained from the difference patterns of data sets collected at $T = 2$ K (where the magnetic order is fully established in both manganates) and well above T_N (that is, at 45 K for $Rb_{11}Mn_8O_{16}$ and at 20 K for $Cs_3Mn_2O_4$). As shown in Fig. 6, several magnetic reflections could be observed in the 2θ range up to 63°.

In the case of $Rb_{11}Mn_8O_{16}$ these reflections appeared at positions with h, k = odd and $\ell = 8$, which are forbidden in the space group $F222$, which allows only reflections with $hk\ell$ values either all *even* or all *odd*. The magnetic reflections can be generated by the rule $(hk\ell)_M = (hk\ell)_N \pm \boldsymbol{k}$, where the propagation vector is $\boldsymbol{k} = (0,0,1)$. This indicates that the magnetically ordered manganese moments in the equivalent positions (0,0,0; 1/2,1/2,0; 1/2,0,1/2; 0,1/2,1/2) + x,y,z of

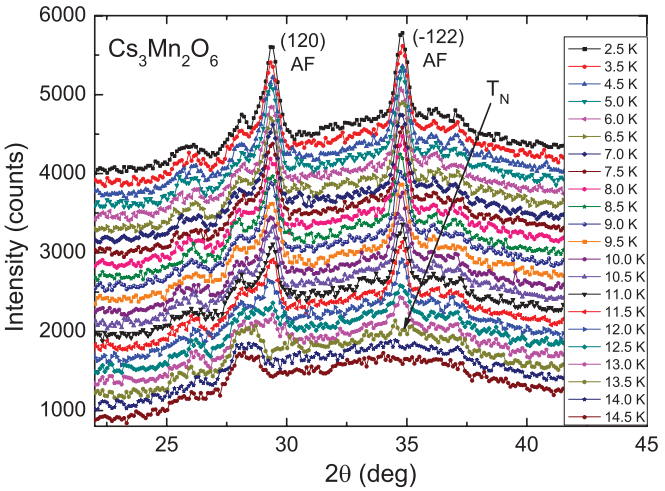

FIG. 5. (Color online) Neutron powder patterns of $Cs_3Mn_2O_4$ collected in the temperature range between 2 and 15 K. Antiferromagnetic ordering of the Mn atoms sets in at the Néel temperature $T_N = 13.5(5)$ K.

the face-centered (F) unit cell show the sequence $++--$. Since magnetic reflections only appear for $(hk\ell)$ with $\ell = 8$, we conclude that the c-axis parameter of the magnetic unit cell is $1/8$ of that of the nuclear cell, so that the moments form the sequence $+-+-$ along the c axis. Rietveld refinements of the magnetic structure confirmed this antiferromagnetic structure.

Since the unit cell of the crystal lattice $Rb_{11}Mn_8O_{16}$ contains 128 (17 structurally different) Mn ions, and magnetic intensity was observable only at the position of seven magnetic Bragg reflections (Fig. 6), it was not possible to determine the magnetic moments for each of these Mn ions individually.

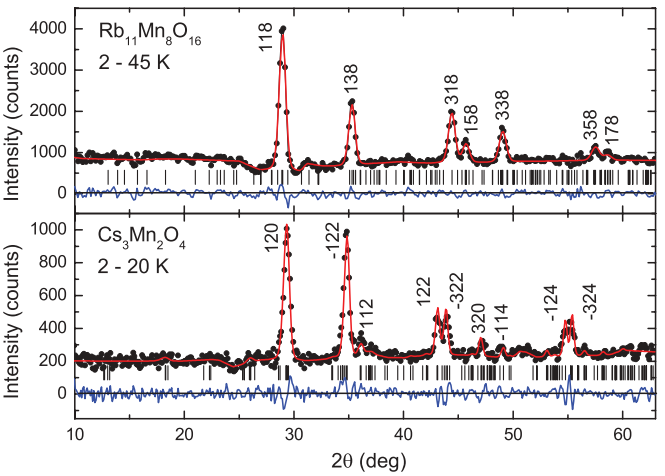

FIG. 6. (Color online) Neutron powder patterns taken with neutron wavelength $\lambda = 2.42$ Å, showing the magnetic intensities of $Rb_{11}Mn_8O_{16}$ and $Cs_3Mn_2O_4$. These difference patterns were obtained by subtracting the data collected well below (at 2 K) and above the Néel temperature, namely, $T = 45$ K ($Rb_{11}Mn_8O_{16}$) and $T = 20$ K ($Cs_3Mn_2O_4$), respectively. The calculated pattern (red) is compared with the observed one (black circles). The difference pattern (blue) as well as the peak positions (black bars) of the magnetic reflections are given in the lower part of each diagram.

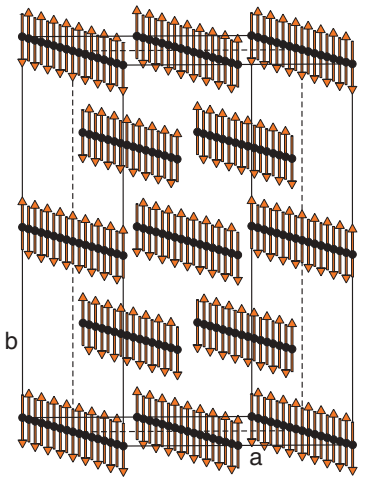

FIG. 7. (Color online) Antiferromagnetic ordering of the manganese ions in $Rb_{11}Mn_8O_{16}$ at $T = 2$ K. The manganese ions form antiferromagnetic chains along the c axis.

In the refinements, all manganese moment amplitudes were therefore constrained to be equal. The best fit was obtained for a structure in which the magnetic moments of the Mn ions in the antiferromagnetic chains along the c axis are aligned parallel to the b axis (Fig. 7). The averaged magnetic moment was found to be $\mu_{av}(\mathrm{Mn}) = 2.83(3)\mu_B$. The refinement resulted in a residual $R_M = 0.051$ (defined as $R_M = \sum |I_{obs} - I_{cal}| / \sum I_{obs}$).

Additional intensity was also found for $T \leqslant 140$ K at the position of the reflections (220) and (040) (Fig. 4), but these intensities do not show any anomaly at T_N. Refinement of the magnetic structure based on difference patterns using the data sets collected at 45 and 200 K yielded a reasonable fit in terms of a model structure where the magnetic moments are aligned ferromagnetically with a moment direction parallel to the a axis, resulting in a magnetic moment of $\mu(\mathrm{Mn}) = 1.7(1)\mu_B$. However, this structure model also generates magnetic intensity on the position of the reflection (260), which is not noticeable in the difference pattern (45–200 K). Moreover, the uniform susceptibility (Fig. 2) does not show any indication of ferromagnetic correlations. We therefore conclude that the additional transition observed at 140 K cannot be ascribed to the onset of ferromagnetic ordering. Possibly a structural rearrangement sets in at this temperature. Further investigations are required to understand the origin of this transition.

In the case of $Cs_3Mn_2O_4$, magnetic intensity was observed for Bragg reflections with $h =$ odd and $k,\ell = 0, 2$, and 4, which are allowed in the space group $P2_1/c$. The propagation vector of the magnetic structure is therefore $\boldsymbol{k} = 0$. The strongest magnetic intensities were observed for reflections with $k = 2$ (Fig. 6), which implies that the b-axis parameter of the magnetic unit cell is $1/2$ of that of the nuclear cell. The magnetic moments of the Mn atoms thus form the sequence $+-+-$ along the b axis (Fig. 8). The $h =$ odd and $\ell =$ even indices of the magnetic reflections indicate antiferromagnetic coupling of the Mn atoms along the a axis, and ferromagnetic coupling along the c axis. With this model, we successfully refined the magnetic structure. The best fit was obtained when

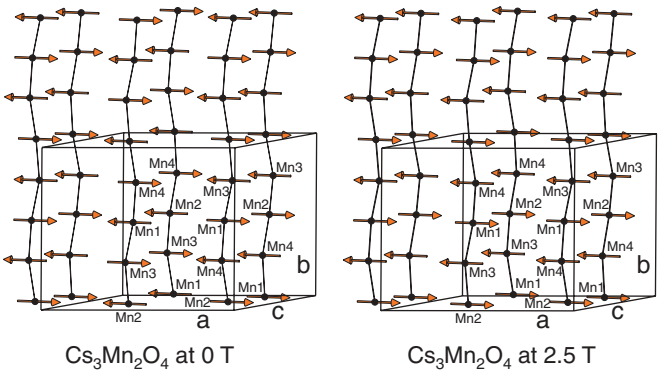

FIG. 8. (Color online) Magnetic ordering pattern of the manganese ions in $Cs_3Mn_2O_4$ at 2 K. The ions labeled Mn1 and Mn2 (Mn3 and Mn4) are in the valence state 3+ (2+). The manganese atoms form antiferromagnetic chains along the b axis. In zero field the interchain coupling is ferromagnetic along the c axis, while it is antiferromagnetic along the a axis. With increasing field the antiferromagnetic coupling changes to a ferromagnetic one, so that in high-field ferromagnetic layers are formed perpendicular to the b axis.

the magnetic moments were aligned within the monoclinic plane perpendicular to the Mn-chain direction, which subtends angles of 23.7(1.7)° and 94.7(1.7)° with the a axis and c axis, respectively (Fig. 8). The average magnetic moment per manganese ion obtained from the refinements was $\mu_{av}(Mn) = 2.987(15)\mu_B$. Since only four different Mn atoms are found in the unit cell, we could subsequently refine the magnetic moments of the Mn^{2+} and Mn^{3+} ions individually, which resulted in a slight improvement of the residual ($R_M = 0.0854$). The magnetic moments obtained in this way were $\mu(Mn^{2+}) = 3.43(11)\mu_B$ and $\mu(Mn^{3+}) = 2.65(10)\mu_B$. Since these moments are antiferromagnetically aligned along the chains, the magnetic structure of this compound can therefore be viewed as an array of antiferromagnetically coupled ferrimagnetic chains (Fig. 8).

Finally, from all the powder patterns collected from 2 K up to the Néel temperature and their refinements we could extract the magnetic moments for both $Rb_{11}Mn_8O_{16}$ and $Cs_3Mn_2O_4$ at each temperature. The results are presented and compared in Fig. 9. As expected, in view of their formal Mn charges, the low-temperature averaged ordered moment of $Cs_3Mn_2O_4$ [$\mu_{av}(Mn) = 2.987(15)\mu_B$] is somewhat larger than the one of $Rb_{11}Mn_8O_{16}$ [$\mu_{av}(Mn) = 2.83(3)\mu_B$].

C. Field-induced magnetic structure of $Cs_3Mn_2O_4$

In view of the field dependence of the uniform magnetization of $Cs_3Mn_2O_4$ (Fig. 3), we carried out neutron powder diffraction studies under different selected applied magnetic fields. Figure 10 shows that the magnetic intensities are strongly modified by external fields up to $H = 2.5$ T, in agreement with the uniform susceptibility. The intensities of the strongest zero-field magnetic reflections (120) and (−122) progressively decrease as the applied field increases, and they disappear completely at 2.5 T. At the same time, new strong magnetic intensities progressively appear at the positions of the reflections (020), (012) [or (210)], (220) [or (022)],

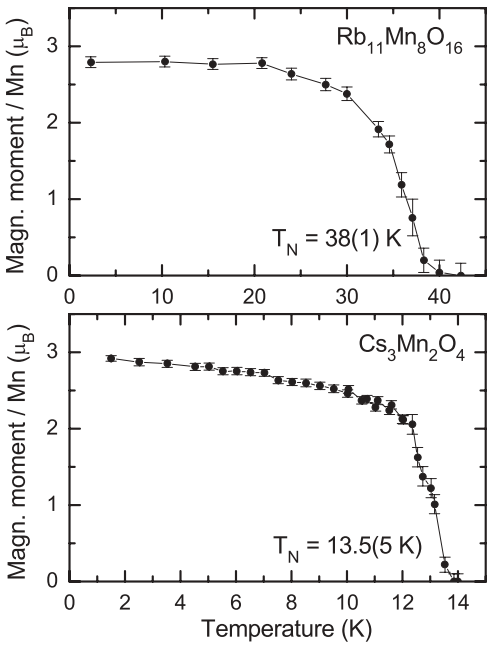

FIG. 9. Temperature dependence of ordered magnetic moments of $Rb_{11}Mn_8O_{16}$ and $Cs_3Mn_2O_4$ as obtained from neutron powder diffraction.

and (−222). The presence of the reflection (020) indicates ferromagnetic alignment within the monoclinic ac plane. This means that the magnetic field reverses the ferrimagnetic moments of every second manganese chain (Fig. 8), so that these moments are ferromagnetically aligned for $H = 2.5$ T. With this model, we obtained a very satisfactory fit of the high-field diffraction pattern, as shown in Fig. 10. The refinement also showed that the magnetic ordering pattern within the Mn chains remains unchanged, and that the moments remain aligned perpendicular to the chain direction.

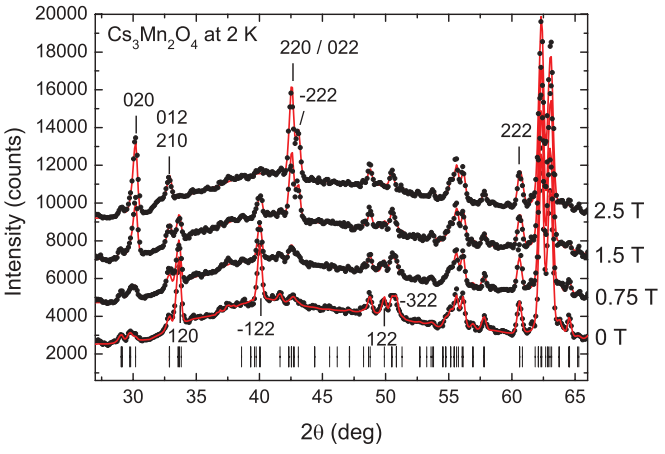

FIG. 10. (Color online) Neutron powder patterns of $Cs_3Mn_2O_4$ at 2 K and magnetic fields $0 \leqslant H \leqslant 2.5$ T. The neutron wavelength was $\lambda = 2.795$ Å. Both nuclear and magnetic Bragg peaks are present. The $hk\ell$ values are given for the reflections where additional magnetic intensities could be observed. The calculated patterns (red) are compared with the observed ones (black circles). The positions of the Bragg peaks (black bars) are given in the lower part of each diagram.

For lower magnetic fields a mixture of the zero-field and high-field magnetic structures is detected (Fig. 10).

Due to the coaligned moments of the ferrimagnetic chains, the magnetic structure present for $H = 2.5$ T exhibits a net ferromagnetic component moment of amplitude $\mu(Mn^{2+}) - \mu(Mn^{3+}) = 0.78\mu_B$ oriented perpendicular to the b axis (Fig. 8). This value is larger than the net moment obtained from the magnetization measurements (Fig. 3), which is reduced due to powder averaging of the moment orientation.

IV. CONCLUSIONS

Our neutron powder diffraction study has allowed us to elucidate the magnetic structures of $Cs_3Mn_2O_4$ and $Rb_{11}Mn_8O_{16}$, which exhibit rare cases of Mn^{2+}-Mn^{3+} charge order with minimal substitutional disorder. Both compounds show magnetic long-range order with antiferromagnetically ordered Mn moments along the MnO_2 chains at low temperatures. Their temperature dependent magnetic susceptibilities, combined with the low Néel temperatures, indicate quasi-one-dimensional exchange Hamiltonians with dominant antiferromagnetic interactions along the chains. The higher T_N displayed by $Rb_{11}Mn_8O_{16}$, as compared to the one of $Cs_3Mn_2O_4$, can be ascribed to the presence of a higher number of Mn ions in neighboring chains at short distances d. For instance, there are ten Mn neighbors with $d \leqslant 6.10$ Å in $Rb_{11}Mn_8O_{16}$, compared to one or two in $Cs_3Mn_2O_4$.

The strong reduction of the sublattice magnetization in the antiferromagnetically ordered phases, compared to the moment values expected for high-spin ions Mn^{3+} and Mn^{2+} with four and five unpaired electrons, respectively, is probably at least in part due to quantum zero-point fluctuations in the quasi-one-dimensional network of exchange bonds. In view of the short Mn-Mn distances along the MnO_2 chains [d(Mn-Mn) = 2.76 and 2.79 Å in $Cs_3Mn_2O_4$, and 2.64 Å $\leqslant$ d(Mn-Mn) $\leqslant$ 2.78 Å in $Rb_{11}Mn_8O_{16}$], which are not much larger than the atomic separation in metallic manganese, it is conceivable that charge delocalization and strong Mn-O covalency also contribute to the moment reduction. Related effects have been observed in other compounds with quasi-one-dimensional exchange interactions made up of edge-linked MX_4 tetrahedra (Ref. 21), such as FeX_2 chain compounds (X = S and Se).[22]

For $Rb_{11}Mn_8O_{16}$ we only provide a simplified description of the magnetic structure, because the complexity of its crystal structure forced us to assume an idealized crystal structure model where all Mn ions had the same charge. In the case of $Cs_3Mn_2O_4$, we were able to determine the ordered moments of Mn^{2+} and Mn^{3+} sublattices separately, and found that they are ferrimagnetically oriented along the chains, resulting in a net magnetic moment of every chain. Whereas these net moments are antiferromagnetically oriented in zero field, a sufficiently intense magnetic field forces them to align ferromagnetically. These experimental results confirm density functional calculations according to which the energy difference between these two states is very small (2.53 meV per unit cell).[13] The metamagnetic transition between both states is presumably responsible for the step in the low-temperature isothermal magnetization between 1 and 2.5 T (Fig. 3). The additional step at very low fields (and the smooth upturn of the magnetization upon cooling in the paramagnetic state shown in Fig. 2) may reflect a subtle spin canting that is not apparent in the neutron diffraction data. A similar effect may be responsible for the slight hysteresis and nonlinearity of the magnetization curve of $Rb_{11}Mn_8O_{16}$ (Fig. 3), and for the increase in magnetization observed upon cooling below T_N in fixed field (Fig. 2).

ACKNOWLEDGMENT

M.A.S.R. is grateful for support from Ministerio de Economía y Competitividad MINECO (Spain) under project FEDER MAT2010-21342-C02-01.

[1] J. Bobroff, N. Laflorencie, L. K. Alexander, A. V. Mahajan, B. Koteswararao, and P. Mendels, Phys. Rev. Lett. **103**, 047201 (2009).
[2] A. Suchaneck, V. Hinkov, D. Haug, L. Schulz, C. Bernhard, A. Ivanov, K. Hradil, C. T. Lin, P. Bourges, B. Keimer, and Y. Sidis, Phys. Rev. Lett. **105**, 037207 (2010).
[3] A. Prodi, E. Gilioli, A. Gauzzi, F. Licci, M. Marezio, F. Bolzoni, Q. Huang, A. Santoro, and J. W. Lynn, Nature Mater. **3**, 48 (2004).
[4] M. Sofin, E.-M. Peters, and M. Jansen, J. Solid State Chem. **178**, 3708 (2005).
[5] P. Horsch, M. Sofin, M. Mayr, and M. Jansen, Phys. Rev. Lett. **94**, 076403 (2005).
[6] M. Raichle, M. Reehuis, G. Andre, L. Capogna, M. Sofin, M. Jansen, and B. Keimer, Phys. Rev. Lett. **101**, 047202 (2008).
[7] N. Z. Ali, J. Sirker, J. Nuss, P. Horsch, and M. Jansen, Phys. Rev. B **84**, 035113 (2011).
[8] J. Nuss, U. Wedig, and M. Jansen, Z. Kristallogr. **226**, 627 (2011).
[9] S. Pfeiffer and M. Jansen, Z. Anorg. Allg. Chem. **633**, 2558 (2007).
[10] S. Pfeiffer, J. Nuss, and M. Jansen, Z. Kristallogr. – New Cryst. Struct. **224**, 377 (2009).
[11] S. Pfeiffer, J. Nuss, and M. Jansen, Z. Anorg. Allg. Chem. **636**, 23 (2010).
[12] J. Nuss, S. Pfeiffer, S. van Smaalen, and M. Jansen, Acta Crystallogr. Sect. B: Struct. Sci. **66**, 27 (2010).
[13] J. Nuss, M. A. Señaris-Rodriguez, P. L. V. K. Dasari, M. Stahl, and M. Jansen, J. Am. Chem. Soc. **134**, 11734 (2012).
[14] D. Trinschek and M. Jansen, Angew. Chem., Int. Ed. **38**, 133 (1999).
[15] M. Jansen, Z. Anorg. Allg. Chem. **638**, 1910 (2012).
[16] A. Möller, P. Amann, V. Kataev, and N. Schittner, Z. Anorg. Allg. Chem. **630**, 890 (2004).
[17] M. M. Thackeray, W. I. F. David, P. G. Bruce, and J. B. Goodenough, Mater. Res. Bull. **18**, 461 (1983).
[18] J. Rodríguez-Carvajal, FULLPROF: A Program for Rietveld Refinement and Pattern Matching Analysis, Abstract of the Satellite Meeting on Powder Diffraction of the XV Congress of the IUCr, Toulouse, France (1990), p. 127.

[19]V. F. Sears, in *International Tables of Crystallography*, edited by A. J. C. Wilson (Kluwer, Dordrecht, 1992), Vol. C, p. 383.
[20]P. J. Brown, in *International Tables of Crystallography*, edited by A. J. C. Wilson (Kluwer, Dordrecht, 1992), Vol. C, p. 391.
[21]D. Welz and M. Nishi, Phys. Rev. B **45**, 9806 (1992).
[22]W. Bronger, A. Kyas, and P. Müller, J. Solid State Chem. **70**, 262 (1987).